View metadata, citation and similar papers at core.ac.uk

brought to you by CORE

provided by UCL Discovery

Thin Solid Films 597 (2015) 19–24

Contents lists available at ScienceDirect

Thin Solid Films

journal homepage: www.elsevier.com/locate/tsf

Improving efficiency of electrostatic spray-assisted vapor deposited $Cu_2ZnSn(S,Se)_4$ solar cells by modification of Mo/absorber interface

Giovanni Altamura, Mingqing Wang, Kwang-Leong Choy *

UCL Institute for Materials Discovery, University College London, Roberts Building, Malet Place, London WC1E 7JE, United Kingdom

ARTICLE INFO

Article history:
Received 20 July 2015
Received in revised form 27 October 2015
Accepted 11 November 2015
Available online 12 November 2015

Keywords:
ZnO
ESAVD
Photovoltaic
$Cu_2ZnSn(S,Se)_4$
Interface

ABSTRACT

Electrostatic spray-assisted vapor deposition (ESAVD) is a non-vacuum, low cost and eco-friendly method to produce $Cu(In,Ga)Se_2$ and $Cu_2ZnSn(S,Se)_4$ (CZTSSe) absorbers for thin film solar cells, and it is a very promising method for industrialization due to it is high deposition speed and close to unity deposition efficiency. In this work, in order to improve the efficiency of ESAVD deposited CZTSSe solar cells, an ultrathin ZnO (circa 10 nm) layer was employed as an intermediate layer between CZTSSe and Mo back contact to avoid the direct contact between Mo and CZTSSe and reduce the decomposition of CZTSSe during annealing process. XRF and EDX were used to characterize the chemical composition of CZTSSe before and after selenization respectively. SEM and Raman results showed the improved absorber morphology and the reduced direct interfacial reaction between CZTSSe and Mo. The improvement of the CZTSSe/Mo interface due to the intermediate layer was also reflected in the quality of the derived photovoltaic devices, leading to an improved efficiency of ESAVD-deposited kesterite solar cells from 3.25% to 4.03%.

© 2015 Elsevier B.V. All rights reserved.

1. Introduction

Kesterite Cu_2ZnSnS_4 (CZTS), $Cu_2ZnSnSe_4$ (CZTSe) and $Cu_2ZnSn(S_xSe_{1-x})_4$ (CZTSSe) are promising candidates for low-cost and high-efficiency earth abundant, thin film solar cells. [1–2]. These absorber materials have direct band gap energies ranging from 1.0 eV [3] to 1.5 eV [4], and high absorption coefficients ($>10^4$ cm^{-1}) [4] making CZTSSe a feasible option for photovoltaic thin film technologies. Moreover, CZTSSe-based materials consist of non-critical elements, therefore they should not suffer from cost and availability limitations [5]. Numerous investigations have been made to improve the photovoltaic performances of kesterite solar cells and develop low-cost manufacturing processes. Different from $Cu(In,Ga)Se_2$ (CIGS) solar cells, for which the vacuum processed devices show much better efficiency than non-vacuum processed ones, solution processed CZTS solar cells show both better performance and lower cost than vacuum processed ones. Hydrazine is a carbon and oxygen-free chemical that can dissolve various binary metal selenides or sulfides with additional Se/S elements. Researchers from IBM reported CZTSSe solar cell with a record conversion efficiency of 12.7% by spin coating the hydrazine slurry [2]. Concerns about the toxicity and flammability of hydrazine limit the scale up of this method. Except for hydrazine, many other solvents such as alcohols [6], 2-methoxyethanol [7], ethylene glycol [8], and dimethyl-sulfoxide (DMSO) [9]were also employed as solvent in CZTS solar cells. DMSO can act as a Lewis base and complex with metal ions either through the oxygen atom or sulfur atom, solar cells using DMSO as a solvent has reached 8% [10]. Spin coating is a widely used method to coat the absorber film in the above wet chemical method, but the high material consumption and long processing times of spin coating method restricts its application in large area industry production. With the fast efficiency improvement of CZTSSe solar cells reported recently, it is essential to develop a deposition method which is compatible with commercialization. In our group, a non-vacuum, low cost and eco-friendly ESAVD method has been adopted to produce CIGS and CZTSSe absorbers for thin film solar cells. ESAVD is a very promising method for industrialization due to its high deposition speed and close to unity deposition efficiency. In our previous work, ESAVD deposited CZTSSe solar cell with efficiency of 1% has been achieved when 2 methoxyethanol was chosen as solvent [8]. In this work, DMSO with good complex with metal salts was adopted as solvent for CZTSSe precursors to better control the composition in the ESAVD deposited absorber. Except for composition and crystallization of absorber, the interface between absorber and Mo glass also has essential effect on the device performance CZTSSe solar cells.

Scragg et al. [11] have reported experimental evidence for the existence of a decomposition reaction of selenium-free CZTS at the interface between CZTS and Mo back contact, which leads to the formation of secondary phases and a thick resistive MoS_2 phase between the absorber and the back contact. The authors demonstrated that high sulfur pressure during annealing influences both surface and back contact decomposition, which could also be correlated to device performances [11]. Lopez-Marino et al. [12] reported the analysis of the decomposition reaction of sulfur-free CZTSe compounds at the interface with Mo back contact under standard annealing conditions. The authors demonstrated that it is possible to inhibit this decomposition reaction, in the case

* Corresponding author.
E-mail address: k.choy@ucl.ac.uk (K.-L. Choy).

http://dx.doi.org/10.1016/j.tsf.2015.11.027
0040-6090/© 2015 Elsevier B.V. All rights reserved.

of selenide kesterite, by using a 10 nm ZnO intermediate layer that is deposited between the Mo-coated substrates and the absorber precursor. The existence of a ZnO nanolayer on the Mo inhibits the CZTSSe decomposition reaction because it prevents direct contact between the absorber and the back contact during selenization step. This leads to a significant improvement in the interface morphology and hence of the photovoltaic performances of the solar cell. These findings have motivated us to explore how this ultrathin ZnO intermediate layer can influence the formation of secondary phases at Mo back contact in the case of sulfo-selenide based kesterites synthesized by a two-step selenization process, where absorbers are deposited by ESAVD method [13]. A combination of different analysis tools, including scanning electron microscopy (SEM), Energy dispersion X-ray analysis (EDX), and Raman spectroscopy have been used to characterize structure, composition and back contact interface of the kesterite absorber. Finally, a correlation between the material analysis and the photovoltaic performances of Mo/CZTSSe/CdS/i-ZnO/Al:ZnO/Ni/Al solar cell is established.

2. Experimental

2.1. Substrate preparation

A 550 nm Mo coated-soda lime glass ($R_{\square} = 0.63\ \Omega/\square$) was used as the standard substrate and was deoxidized for 10 s in a 10% NH_3 solution. Out of this, two types of sample were prepared: sample A and sample B. Sample A has a standard back contact. For sample B, 10 nm of i-ZnO was deposited onto the Mo substrate by magnetron sputtering deposition (HHV 500 Auto vacuum coater, 1.0 W/cm^2, 10^{-3} mbar, 6 sccm Ar and 2 sccm O_2, room temperature, 15 min) using 99.99% purity i-ZnO target (Kurt Lesker). The thickness of the as-deposited ZnO nanolayer has been checked by Bruker Dektak XT contact profilometer with a 5% absolute accuracy.

2.2. Precursor preparation

An environmentally friendly and sustainable ESAVD process has been exploited for the process of CZTSSe absorber layers [13]. Pure CZTS films were deposited from a mixed solution containing $Cu(OAc)_2$, $ZnCl_2$, $SnCl_2$, and thiourea in DMSO. The deposition was performed at a temperature range of 250–350 °C. The composition of the precursor was tailored to give a Zn-rich and Cu-poor absorber which has proved to give the best photovoltaic efficiency at the device level [2]. Elemental composition for both samples has been measured by X-ray fluorescence (Fischerscope XAN 250) and summarized in Table 1.

2.3. Selenization

The as-deposited CZTS layers was first annealed in a tubular furnace at 300 °C for 15 min using 120 mg SnS, and subsequently selenized at 550 °C for 30 min in a dedicated graphite box in order to form the final CZTSSe absorber (Fig. 1).

Table 1
Elemental composition (atomic percentage with 1% relative error) of the as-deposited CZTS absorber in sample A and sample B. Results are obtained from top-view XRF measurements.

	Sample A	Sample B
[Cu]	19.09%	19.62%
[Zn]	15.25%	15.36%
[Sn]	14.02%	13.48%
[S]	52.13%	52.01%
[Cu]/[Zn + Sn]	0.65	0.68
[Zn]/[Sn]	1.08	1.1
[S]/[Cu + Zn + Sn]	1.07	1.07

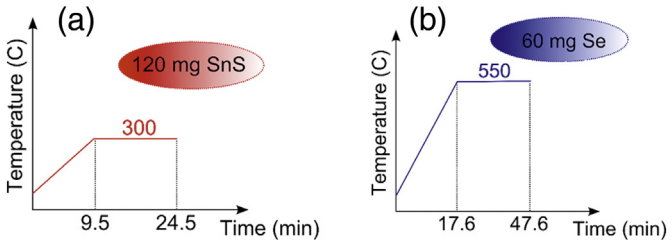

Fig. 1. Schematic diagram of the selenization process annealing under SnS atmosphere (a) followed by annealing under Se atmosphere (b) and natural cooling.

2.4. Device fabrication

After selenization, circa 50 nm thick of CdS layer was deposited on top of the CZTSSe absorber using chemical bath deposition (CBD) method. On top of the CdS, a bilayer composed of i-ZnO(50 nm) and Al:ZnO (450 nm) was sputtered as the window layer. Intrinsic ZnO was deposited using the same conditions as before. Al:ZnO was deposited by RF-sputtering (HHV 500 Auto vacuum coater, 1.1 W/cm^2, 10^{-3} mbar, for 77 min in Ar atmosphere, using 99.99% purity i-ZnO and 2% Al-doped ZnO targets. Finally, patterned Ni/Al layer was thermally evaporated on top of the window layer as finger electrodes. The dimension of an individual solar cell was 4×4 mm^2.

2.5. Characterization

Raman measurements were carried out using Horiba Jobin-Yvon LabRam spectrometer with green laser (514 nm) excitation. The surface morphology of the films and its composition were characterized by FEI XL-30 scanning electron microscopy, energy dispersive X-Ray analysis (EDX), and X-Ray fluorescence analysis (XRF) respectively. The performance of the solar cells were evaluated under AM1.5 simulated solar light with intensity of 100 mW/cm^2 using an Oriel Solar 1A.

3. Results & discussions

ZnO intermediate layer has been used mainly because it is readily available in conventional thin film solar cell technology. In the case of Zn, it is a constituent element of CZTSSe, whereas O is replaced during selenization by Se incorporation thus minimizing potential oxygen contamination.

3.1. SEM

Fig. 2 shows top-view and cross-sectional SEM images of samples A and B after selenization. The top-view analysis shows a less compact film for sample A (Fig. 2a) with a grain size that in some cases exceeds 2 μm width, while a more dense film is displayed in Fig. 2b for Sample B with ZnO nanolayer.

The cross-sectional SEM images show two distinguishable zones, for both samples, with large grains on top (Zone 1) and smaller ones (Zone 2) closer to the Mo interface. This two-zone CZTSSe has already been observed in literature for vacuum deposited absorber [14–15]: Zone 1 is typically identified as a CZTSSe layer with big grains and low residual carbon content, while Zone 2 is instead pinpointed as a small crystals CZTSSe layer with high residual carbon content, as demonstrated in other non-vacuum CZTSSe deposition technologies [15–17] and in this work by EDX analysis (not shown here). In Fig. 2d a thin layer of $Mo(S,Se)_2$ can also be observed between the metallic back contact and the absorber, which is in accordance with the literature [18]. It is important to highlight the absence of voids at the absorber back surface which is common in CZTSSe after the selenization step.

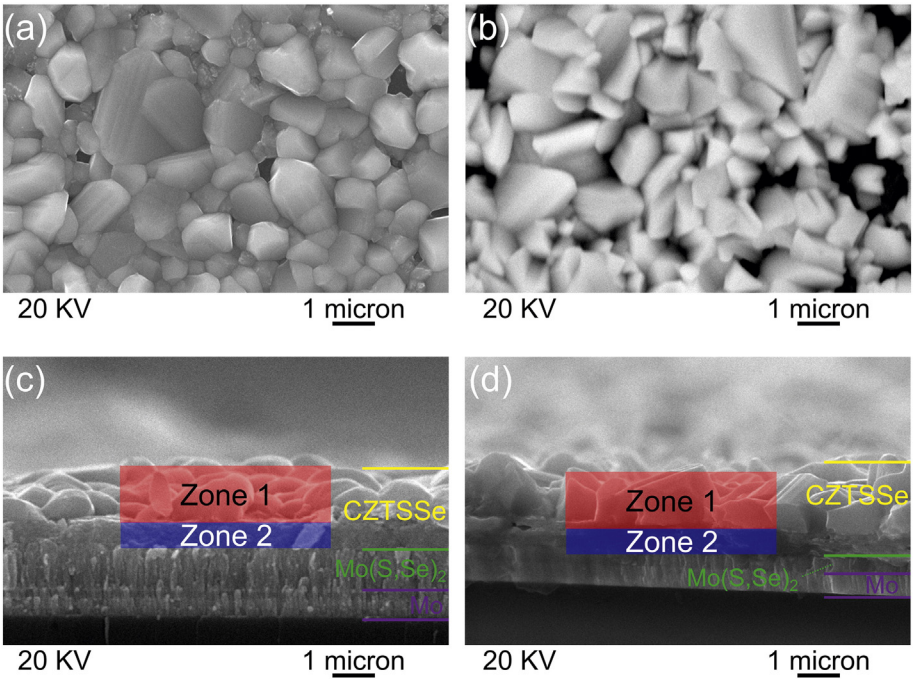

Fig. 2. Top-view and cross-sectional SEM images of CZTSSe after selenization for sample A (a, c) and sample B (b, d).

3.2. EDX

Energy dispersion X-ray measurements, in top-view configuration, at 25 kV, were performed to evaluate compositional changes in the selenized absorber layers. The evaluation of the metal ratios, [Zn]/[Sn] and [Cu] / [Zn + Sn], in the CZTSSe layers is critical since improved performance in solar cells has been attributed to a Cu-poor and Zn-rich absorber layer [1–2]. The results are summarized in Table 2.

As already demonstrated in Table 1, the [Zn]/[Sn] ratio of sample A was a little lower than that of sample B (1.08 vs 1.1) before selenization. The Zn]/[Sn] atomic ratios were calculated over the whole sample, thereby the higher Zn]/[Sn] in sample B should come from the ZnO previously deposited on the Mo. After selenization, the [Cu]/[Zn + Sn] ratio was similar for both samples A and B (0.85/0.81), whereas the [Zn]/[Sn] ratio of sample A (1.25) was much higher than sample B (1.09). Compared with samples before selenization, the [Cu]/[Zn + Sn] ratio of both sample A and sample B increased greatly from 0.65 and 0.68 to 0.85 and 0.81 respectively. The higher [Cu]/[Zn + Sn] ratio after selenization is mainly due to Sn-losses, which typically occurs during selenization because of re-evaporation of the volatile species like SnS–SnSe [19]. The higher value of the Zn/Sn ratio in sample A (without intermediate ZnO layer) than in sample B (with intermediate ZnO layer) suggests a higher loose of Sn during the annealing of the sample without the ZnO intermediate layer. This can be a first demonstration of the beneficial effect of ZnO-nanolayer to prevent decomposition of CZTSe in the vicinity of the Mo back contact which allows also a reduction of the loss of Sn during the annealing. The reduction of Sn-losses might also be due to a more stable CZTSSe limiting the possibility to form volatile Sn-chalcogens phases. An average alloy composition of circa x = 0.16 ([S]/[S + Se]) also indicates that Se replaced S in the absorber during the annealing for both samples (results summarized in Table 2).

Table 2
Elemental composition of sample A and sample B. Results are obtained from top-view EDX measurements.

	Sample A	Sample B
[Cu]/[Zn + Sn]	0.85	0.81
[Zn]/[Sn]	1.25	1.09
[S]/[S + Se]	0.14	0.18

3.3. Raman

Raman spectroscopy is a very useful tool to characterize the presence of minor phases. In order to study the effect of the ZnO layer on reducing the possible decomposition of CZTSSe at the back contact, Raman analysis was performed on the absorber (Fig. 3) and on the back contact after the CZTSSe film being removed mechanically (Fig. 4). Fig. 3 shows Raman spectra of sample A and sample B where the presence of the same peak at 197–202 cm^{-1} could be assigned to the A mode of $Cu_2ZnSnSe_4$ kesterite [17], whereas the peak at 329 cm^{-1} was assigned to Cu_2ZnSnS_4 [20]. This is in good agreement with the bimodal behavior of the CZTSSe alloy already observed by Grossberg et al. [21]. The CZTS A peak was less intense than the CZTSe one due to the low S-content in

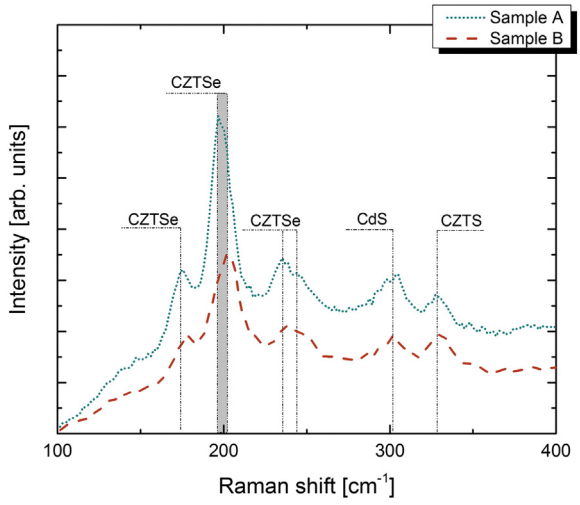

Fig. 3. Raman spectra of selenized CZTSSe absorbers for sample A (dotted) and B (dashed).

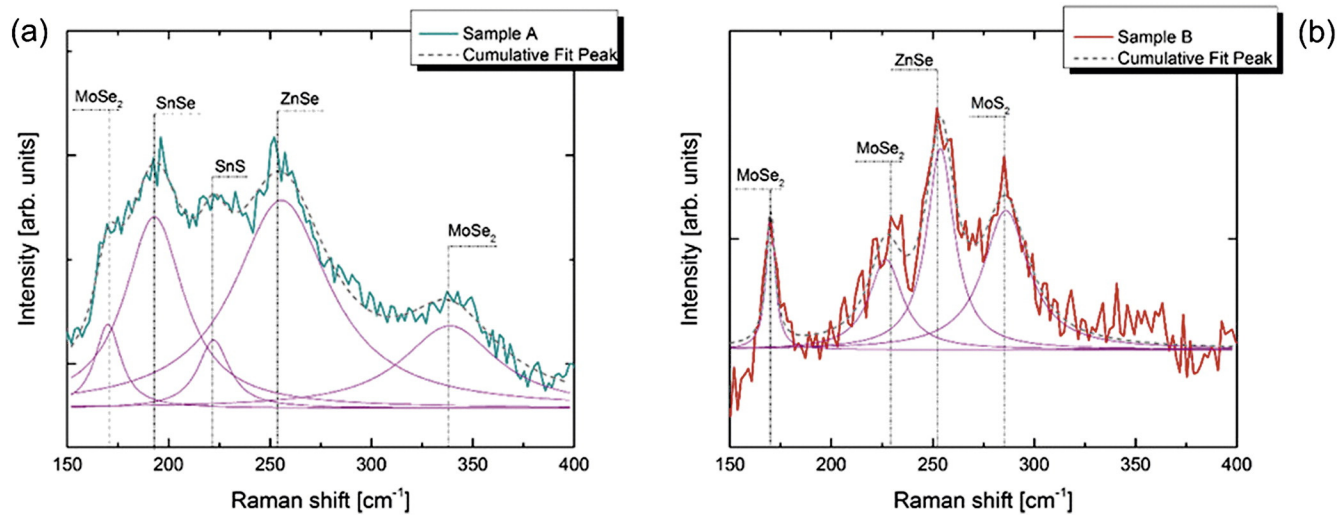

Fig. 4. Raman spectra of the back contact after removal of annealed CZTSSe absorber for samples A and B.

the final absorber, thus confirming the EDX results previously displayed in Table 2. Other peaks of CZTSe were present in the range of 174–176 cm^{-1} and 234–236 cm^{-1} [21]. For both samples, no other secondary phases were detected. The CdS peak encountered at 304 cm^{-1} was from the ultrathin CdS layer deposited on CZTSSe in order to avoid surface oxidation of the absorber prior to Raman analysis.

In order to determine the effect of the ZnO intermediate layer in detail, especially on the CZTSSe decomposition at the back contact, a lift-off of the absorber was performed and Raman scattering was employed to examine the front surface of the Mo back contact. In order to avoid uncertainties associated with the lift-off of the absorber, both the substrate front surface and the CZTSSe back absorber region of the removed samples were analyzed (Fig. 4). Since neither the CZTSSe characteristic peaks on the back contact, nor the $Mo(S,Se_)_2$ peaks on the back surface of the absorber were identified, we could assess that the films were removed at the interface between $Mo(S,Se)_2$ and CZTSSe layers.

Fig. 4 shows the Raman spectra of the back contact of the absorber obtained from samples A and B after the removal of the absorber, respectively. The spectrum from sample A was characterized by the presence of a dominant peak at 252 cm^{-1} which agrees with the main peak reported for ZnSe [22]; the main peak at 190 cm^{-1} and weaker contributions at 169 cm^{-1} and 221 cm^{-1} has been identified with the vibrational mode of binary SnS [23–24]. It is important to note that due to the Zn-rich conditions used in these films (as confirmed by EDX in Table 2), the probability to form Zn-based binary phases is likely. However, for Cu-poor conditions used in the absorbers, the likelihood for the appearance of binary/ternary Cu-based phases is expected to be very low. Raman shift at 340 cm^{-1} was also visible and can be referred to a $MoSe_2$ phase [25]. Raman shifts in Fig. 4(a) suggest that the surface of the back contact of Sample A was mainly constituted of $MoSe_2$, with the presence of some minor phases. The Raman spectrum of Sample B, however, shows $MoSe_2$ (169 cm^{-1}, 229 cm^{-1}) and MoS_2 (285 cm^{-1}) [11] as dominant peaks. The appearance of the MoS_2 phase in sample B was in accordance with the EDX results showing a higher chalcogens ratio [S]/[S + Se]. Another noticeable Raman shift has been seen for the ZnSe peak at 252 cm^{-1}. This analysis demonstrates that ZnO deposited by sputtering (sample B) was less likely to promote the formation of undesirable minor phases like SnS or SnSe (predicted bandgap lower than the one of CZTSSe).

3.4. I–V measurement

Following material characterization, samples A and B were employed in full PV devices. At least twelve 0.16 cm^2 solar cells have been fabricated and electrically characterized for each sample. As shown in Fig. 5, photovoltaic properties of an average value of 20 pixel cells were depicted. As already demonstrated for pure CZTS [11] and CZTSe [12] solar cells, the median power conversion efficiency (PCE), shown in Fig. 5a in the case of solar cells with an intermediate layer (10 nm ZnO, sample B), was higher (3.52%) as compared to the reference cells processed without ZnO intermediate layer (2.81%). The variation of PCE between cells containing different samples is clearly dominated by the variation of the fill factor (FF) (Fig. 5b). This result demonstrated the beneficial effect of the proposed ZnO interfacial layer to improve the quality of the interface between the CZTSSe and the $Mo(S,Se)_2$ layer formed on the top of the back contact. In order to check the possible implications of parasitic resistances in the FF, dark J-V measurements were conducted. PCE gain in the case of sample B was mainly due to the significant reduction of the series resistance (results not shown here) and the consequent increase of the Jsc (Fig. 65d) and FF values (Fig. 6b). Three factors could be responsible for the decrease of the Rs in sample B: (i) reduction of voids at the interface between CZTSSe and Mo, although no apparent evidence have been found through SEM images, (ii) possible reduction of the ZnSe phase amount in the final absorber compared to sample A [26] as demonstrated by EDX of lower Sn loss after selenization in sample B (Table 2) is responsible for R_s variations, and (iii) better CZTSSe absorber quality as demonstrated by the lower full width at half maximum of the main CZTSe Raman peak at 197 cm^{-1} in the case of sample B compared to that of sample A. Based on the scientific evidences showed in the manuscript, both of the last two reasons play a part in this case. There was also an insignificant increase of the V_{oc} (0.2% relative value) in sample B as illustrated in Fig. 6c.

The light J-V characteristics of the two best performing cells are displayed in Fig. 6. The best sample A-based solar cell showed PCE of 3.25%, FF of 42.8%, Voc of 0.29 V, and Jsc of 26.9 mA/cm^2 respectively, whereas the sample B-counterpart demonstrated PCE of 4.03%, FF of 43.4%, Voc of 0.31 V, and Jsc of 29.9 mA/cm^2 respectively. Above Photovoltaic results illustrated once again the importance of a ZnO intermediate layer between the CZTSSe absorber and the Mo back contact on device performance improvement.

4. Conclusions

In this work, a low cost, scalable ESAVD method using DMSO as solvents was employed to deposit CZTS absorbers. In order to further improve the device efficiency, an ultrathin ZnO intermediate layer was deposited between CZTSSe and Mo to minimize absorber

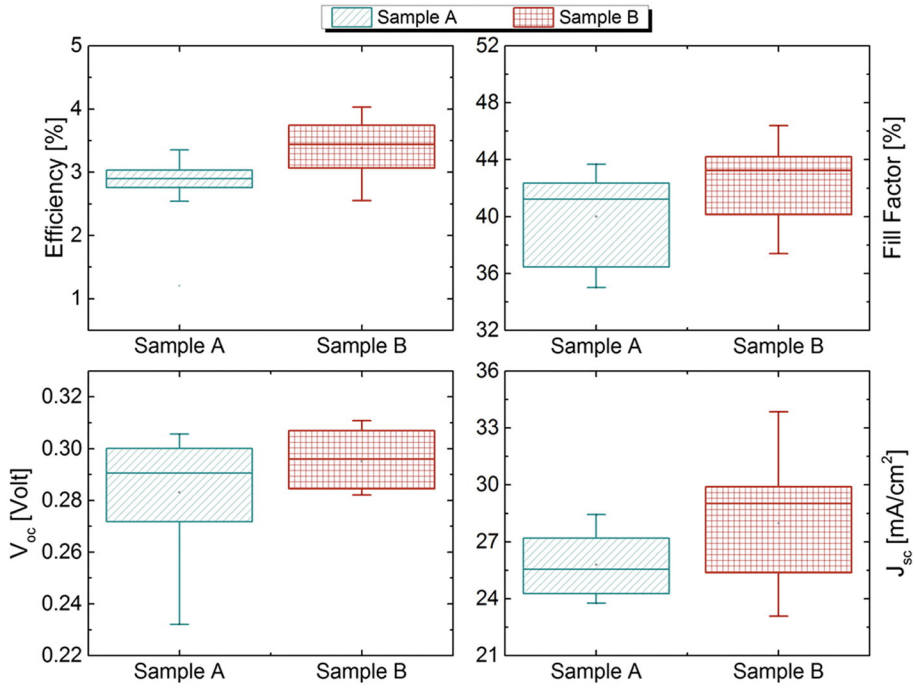

Fig. 5. Current–voltage measurements under illumination of Mo/CZTSSe/CdS/TCO/Ni/Al solar cells: efficiency (a); fill factor (b); open-circuit voltage (c); and short-circuit current (d).

decomposition at the back contact surface. The thin ZnO layer no longer existed after selenization treatment (SEM images in Fig. 2) because Zn was incorporated into the CZTSSe absorber whereas O was replaced by Se. The reaction between ZnO and Se vapor reduced the thickness of high resistance $Mo(S,Se)_2$ layer formed during selenization. For Sample B with a thin ZnO intermediate layer, the Zn/Sn ratio after selenization was lower than reference sample. It can be concluded that preventing decomposition of CZTSe in the vicinity of the Mo back contact allows also a reduction of the loss of Sn during the annealing, which suggests the existence of a relationship between the loss of Sn and the formation of secondary phases at the back region of the absorbers. Comparison between Raman spectrum of sample A and sample B proved that a thin ZnO layer successfully reduced the decomposition of CZTSSe at the back contact surface. The improvement of the CZTSSe|Mo interface due to the intermediate layer was also reflected in the quality of the derived photovoltaic devices leading to an improved efficiency for ESAVD-deposited kesterite of 4.03%.

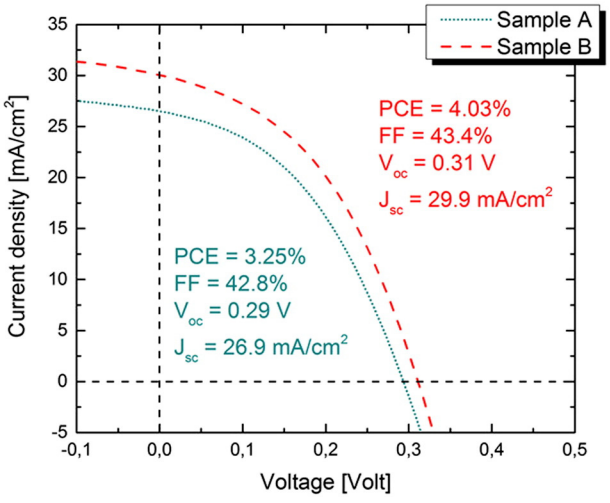

Fig. 6. J–V characteristics of the best-performing Mo/CZTSSe/CdS/TCO/Ni/Al solar cell for sample A (dotted) and sample B (dashed).

Author contributions

The manuscript was written through contributions of all authors. All authors have given approval to the final version of the manuscript.

Funding sources

This work was supported by the EU framework 7 SCALENANO Project, No. NMP4-LA-2011-284486.

Acknowledgments

Dr. Altamura would like to thank James Davy and Dr. Anower Hossein (University College London) for numerous inspiring discussions.

References

[1] H. Katagiri, K. Jimbo, S. Yamada, T. Kamimura, W.S. Maw, T. Fukano, T. Ito, T. Motohiro, Enhanced conversion efficiencies of Cu2ZnSnS4-based thin film solar cells by using preferential etching technique, Appl. Phys. Express 1 (2008) 041201.
[2] W. Wang, M.T. Winkler, O. Gunawan, T. Gokmen, T.K. Todo-rov, Y. Zhu, D.B. Mitzi, Device characteristics of CZTSSe thin-film solar cells with 12.6% efficiency, Adv. Mater. 4 (2014) 7.
[3] S. Ahn, S. Jung, J. Gwak, A. Cho, K. Shin, K. Yoon, D. Park, H. Cheong, J.H. Yun, Determination of band gap energy (Eg) of Cu2ZnSnSe4 thin films: on the discrepancies of reported band gap values, Appl. Phys. Lett. 97 (2010) 021905.
[4] H. Katagiri, K. Saitoh, T. Washio, H. Shinohara, T. Kurumadani, S. Miyajima, Development of thin film solar cell based on Cu2ZnSnS4 thin films, Sol. Energy Mater. Sol. Cells 65 (2001) 141.
[5] C. Wadia, A.P. Alivisatos, D.M. Kammen, Materials availability expands the opportunity for large-scale photovoltaics deployment, Sci. Technol. 43 (2009) 2072.
[6] C.M. Fella, A.R. Uhl, Y.E. Romanyuk, A.N. Tiwari, Cu2ZnSnSe4 absorbers processed from solution deposited metal salt precursors under different selenization conditions, Phys. Status Solidi A 209 (2012) 1043–1048.
[7] K. Tanaka, M. Oonuki, N. Moritake, H. Uchiki, $Cu_2ZnSnS_4Cu_2ZnSnS_4$ thin film solar cells prepared by non-vacuum processing, Sol. Energy Mater. Sol. Cells 93 (2009) 583–587.
[8] Y. Sun, K. Zong, H. Zheng, H. Wanga, J. Liu, H. Yan, M. Zhu, Ethylene glycol-based dip coating route for the synthesis of Cu_2ZnSnS_4 thin film, Mater. Lett. 92 (2013) 195–197.

[9] W. Ki, H.W. Hillhouse, Earth-abundant element photovoltaics directly from soluble precursors with high yield using a Non-toxic solvent, Adv. Energy Mater. 1 (2011) 732–735.
[10] H. Xin, J.K. Katahara, I.L. Braly, H.W. Hillhouse, 8% efficient Cu2ZnSn(S,Se)4 solar cells from redox equilibrated simple precursors in DMSO, Adv. Energy Mater. 4 (2014) 1301823.
[11] J. Scragg, J. Timo Watjen, M. Edoff, T. Ericson, T. Kubart, C. Platzer-Bjorkman, A detrimental reaction at the molybdenum back contact in Cu2ZnSn (S, Se) 4 thin-film solar cells, J. Am. Chem. Soc. 134 (2012) 19330–19333.
[12] S. Lopez-Marino, M. Placidi, A. Perez-Tomas, J. Llobet, V. Izquierdo-Roca, X. Fontane, A. Fairbrother, M. Espındola-Rodrıguez, D. Sylla, A. Perez-Rodrıguez, E. Saucedo, Inhibiting the absorber/Mo-back contact decomposition reaction in Cu 2 ZnSnSe 4 solar cells: the role of a ZnO intermediate nanolayer, J. Mater. Chem. A 1 (2013) 8338–8343.
[13] M. Wang, X. Hou, J. Liu, K.L. Choy, P. Gibson, E. Salem, D. Koutsogeorgis, W. Cranton, An alternative non-vacuum and low cost ESAVD method for the deposition of Cu (In, Ga) Se2 absorber layers, Phys. Status Solidi A 212 (2015) 72–75.
[14] G. Altamura, L. Grenet, C. Bougerol, E. Robin, D. Kohen, H. Fournier, A. Brioude, S. Perraud, H. Mariette, Cu2ZnSn(S1–xSex)4 thin films for photovoltaic applications: influence of the precursor stacking order on the selenization process, J. Alloys Compd. 588 (2014) 310–315.
[15] W. Hsu, B. Bob, W. Yang, C. Chung, Y. Yang, Reaction pathways for the formation of Cu 2 ZnSn (Se, S) 4 absorber materials from liquid-phase hydrazine-based precursor inks, Energy Environ. Sci. 5 (2012) 8564–8571.
[16] Y. Cao, M.S. Denny Jr., J.V. Caspar, W.E. Farneth, Q. Guo, A.S. Ionkin, L.K. Johnson, M. Lu, I. Malajovich, D. Radu, H.D. Rosenfeld, K. Roy Choudhury, W. Wu, High-efficiency solution-processed Cu2ZnSn(S,Se)4 thin-film solar cells prepared from binary and ternary nanoparticles, J. Am. Chem. Soc. 134 (2012) 15644–15647.
[17] M. Dimitrievska, H. Xie, A. Fairbrother, X. Fontané, G. Gurieva, E. Saucedo, A. Pérez-Rodríguez, S. Schorr, V. Izquierdo-Roca, Appl. Phys. Lett. 105 (2014) 031913.
[18] K. Kim, K. Yoon, $MoSe_2$ formation from selenization of Mo and nanoparticle derived Cu(In, Ga)Se2/Mo films, photovoltaic energy conversion, Conference Record of the 2006 IEEE 4th World Conference, 1 2006, pp. 506–508.
[19] P.A. Fernandes, P.M.P. Salomé, A.F. da Cunha, Growth and Raman scattering characterization of Cu_2ZnSnS_4 thin films, Thin Solid Films 517 (2009) 2519–2523.
[20] L. Sun, J. He, H. Kong, F. Yue, P. Yang, J. Chu, Structure, composition and optical properties of Cu_2ZnSnS_4 thin films deposited by pulsed laser deposition method, Sol. Energy Mater. Sol. Cells 95 (2011) 2907–2913.
[21] M. Grossberg, J. Krustok, J. Raudoja, K. Timmo, M. Altosaar, T. Raadik, Photoluminescence and Raman study of Cu2ZnSn(SexS1–x)4 monograins for photovoltaic applications, Thin Solid Films 519 (2010) 7403–7406.
[22] C.G. Munce, G.K. Parker, S.A. Holt, G.A. Hope, A Raman spectroelectrochemical investigation of chemical bath deposited CuxS thin films and their modification, Colloids Surf. A 295 (2007) 152–158.
[23] H.R. Chandrasekhar, R.G. Humphreys, U. Zwick, M. Cardona, Infrared and Raman spectra of the IV-VI compounds SnS and SnSe, Phys. Rev. B 15 (1977) (2177–1977).
[24] X. Fontané, V. Izquierdo-Roca, A. Fairbrother, M. Espindola-Rodriguez, S. Lopez-Marino, M. Placidi, T. Jawhari, E. Saucedo, A. Perez-Rodriguez, Proceedings of the 39th IEEE Photovoltaic Specialists Conference, 2013 2581–2584.
[25] A. Bollero, L. Kaupmees, T. Raadik, M. Grossberg, S. Fernandez, Thermal stability of sputtered Mo/polyimide films and formation of MoSe 2 and MoS 2 layers for application in flexible Cu (In, Ga)(Se, S) 2 based solar cells, Thin Solid Films 520 (2012) 4163–4168.
[26] A. Redinger, K. Hönes, X. Fontané, V. Izquierdo-Roca, E. Saucedo, N. Valle, A. Pérez-Rodríguez, S. Siebentritt, Detection of a ZnSe secondary phase in coevaporated $Cu_2ZnSnSe_4$ thin films, Appl. Phys. Lett. 98 (2011) 101907.